Degradable biporous polymeric networks based on 2-methylene-1,3-dioxepane: Towards hierarchically structured materials meant for biomedical applications

Brian Barber Nunez, Yohann Guillaneuf, Daniel Grande, Benjamin Carbonnier, Benjamin Le Droumaguet

Degradable biporous polymeric networks based on 2-methylene-1,3-dioxepane: Towards hierarchically structured materials meant for biomedical applications

Brian Barber Nunez,[1] Yohann Guillaneuf,[2] Daniel Grande,[1,‖] Benjamin Carbonnier,[1] Benjamin Le Droumaguet[1,*]

[1] *Univ Paris Est Creteil, CNRS, Institut de Chimie et des Matériaux Paris-Est (ICMPE), UMR 7182, 2 rue Henri Dunant, 94320 Thiais, France*

[2] *Aix Marseille Univ, CNRS, Institut de Chimie Radicalaire (ICR), UMR 7233, F-13397 Marseille, France*

[*]Corresponding author: benjamin.le-droumaguet@cnrs.fr

[‖]*Current address : Université de Strasbourg, CNRS, Institut Charles Sadron (ICS), UPR 22, 67034 Strasbourg cedex 2, France*

Abstract:

For the first time, the preparation of doubly porous "poly(e-caprolactone)-like" networks through free-radical ring-opening copolymerization of 2-methylene-1,3-dioxepane with divinyl adipate was achieved *via* a double porogen templating approach. This versatile strategy allowed for the formation of macropores of around 150 µm generated by removal of sieved and sintered NaCl particles in water, while smaller pores in the 1-10 µm range were created by phase separation during the copolymerization process through a syneresis mechanism in the presence of a porogenic solvent. The chemical nature of the as-obtained scaffolds was evidenced by Raman spectroscopy. The two distinct porosity levels could be examined by scanning electron microscopy and mercury intrusion porosimetry. The nature of the porogenic solvent as well as its volume proportion and the amount of crosslinking agent in the polymerization feed allowed for finely tuning the porous features of the micropores. The crucial role of the double porosity of such biporous scaffolds on their water uptake and mechanical properties under compression was assessed by comparing them with their monoporous analogues, while their degradability was investigated in different alkaline aqueous media. The double porosity enabled a synergistic effect regarding the water uptake of the resulting scaffolds when compared to their monoporous counterparts. Doubly porous polymeric materials with appropriate mechanical properties were obtained, possessing high compressibility and shape memory behavior upon consecutive compression cycles. Finally, these materials display degradation rates that could be controlled depending on medium pH.

Keywords: doubly porous polymers, degradable materials, 2-methylene-1,3-dioxepane, water uptake, compressibility

1. Introduction

The human body is constituted of a complex system associated with different tissues that must fulfill specific roles for a proper function of the body. Generally, human tissues have a very limited ability to regenerate themselves, namely by the concentration of cells that reestablish the continuity of the tissue, by forming a scar or by reinitiating the formation process where the injured tissue is regenerated [1]. Although grafting is the most successful treatment, its limitation stems from the scarcity of donor's tissue, immune rejection, and infection. Moreover, as population and life expectancy increase every year, the need for regeneration of diverse tissues also increases. To overcome such shortcomings, tissue engineering has arisen as a multidisciplinary field with the aim of developing artificial functional materials, commonly known as scaffolds, that are capable of regenerating or improving the damage tissue [2]. A suitable scaffold must be biocompatible, biodegradable, and porous with appropriate morphological and mechanical properties. The biocompatibility of such scaffolds is important to allow for a normal wound healing, reconstruction, and tissue integration without severe inflammation that could lead to infection and rejection by the body [3]. Furthermore, biodegradability is crucial as the cells must create a natural matrix while the polymeric chains of the scaffold degrade into simpler metabolizable intermediates through enzymatic action and hydrolysis [4]. In addition, mechanical properties similar to those of the native tissue are essential to support the correct generation of the new cellular matrix through the whole process [5]. In tissue engineering, porous features greatly impact the outcome of the scaffold as it supports cell adhesion and migration, the flow of oxygen and nutrients needed for the cellular process and the flow of metabolic wastes [6]. The latter have shown to be a strongly determining factor on the performance of the material *in vitro* and *in vivo*, as pore size, geometry, alignment and distribution play a crucial role in cell migration, proliferation, and differentiation [6–12]. Although many research studies aim at optimizing the architectural characteristics of new scaffolds, it still remains a challenge.

In recent years, materials presenting dual or multiple porosity levels have shown enhanced performances in cellular response due to the synergic combination of the distinct pore levels where large macropores (>100 μm) improve cell distribution and vascularization [13], while smaller pores (1-10 μm) increase the scaffold permeability, and therefore improve the nutrient adsorption and proliferation of the cells [14]. These materials have been fabricated by different techniques, including solvent casting-particulate leaching [15], phase separation [16], electrospinning [17], gas foaming [18], and 3D printing [19] among others, each one with their own advantages and drawbacks [8]. In this regard, materials prepared by the

combination of particulate leaching and phase separation have shown good control over the pore size where the principal shortcoming is the complete removal of the porogens, especially for the smaller pores [8]. Nevertheless, previous studies from our group [20–22] have demonstrated the successful preparation of well-interconnected biporous materials with independent control over macro- and nanoporosity, achieved without residual porogens. This was accomplished by using Spark Plasma Sintering (SPS) to sinter the macroporogens, an alternative to the traditional thermal sintering of inorganic salts. By using SPS, the contact surface between porogen particles of the salt template is enhanced, thus facilitating the complete removal of porogens at the end of the fabrication process. On the other hand, the (co)polymer from which the scaffolds are made is determinant to fulfill the characteristics of a suitable material for tissue engineering applications. In this regard, polymeric materials have been used extensively in the last decades as their properties can be tuned easily. To this purpose, the most common polymers are poly(ε-caprolactone) (PCL) [23], poly(glycolic acid) (PGA) [24], poly(L-lactic acid) (PLA) [25], and poly(lactic-*co*-glycolic acid) (PLGA) [26], as they possess good stability, low immune response, biocompatible character, tunable degradation rates and mechanical performances [27]. One alternative strategy to these well-studied common polymers has emerged in the last decade, and relies on the (co)polymerization of cyclic ketene acetals (CKAs) for the production of aliphatic/aromatic polyesters by (controlled) free-radical ring opening polymerization ((c)rROP) to prepare biocompatible and biodegradable materials [28]. Especially, 2-methylene-1,3-dioxepane (MDO) can generate "PCL-like" polyesters, *i.e.* presenting the same chemical structure as PCL, upon homopolymerization through (c)rROP.

In the present work, we describe the preparation of novel biodegradable porous polymeric networks constituted of MDO and divinyl adipate (DVA) by a double porogen templating approach showing an independent control of the two porosity scales and good interconnection that were studied by scanning electron microscopy (SEM) and indirectly by water uptake. The macroporosity was generated by using a NaCl template sintered by SPS using sieved salt particles of 250-400 µm, while the smaller porosity was achieved by using *n*-hexane as a porogenic solvent. The effect of dual porosity as well as the variation in crosslinking agent concentration were investigated in terms of its compressive mechanical properties. Degradation of MDO-based materials was carried out to elucidate the stability of the scaffolds in a pH 7.4 phosphate buffer solution mimicking typical serum physiological medium as well as in alkaline accelerated conditions.

2. Experimental

2.1. Materials

Chloroacetaldehyde dimethyl acetal (CADA, 97%), 1-4 butanediol (99%), and Dowex® 50 acidic resin were purchased from Thermo scientific. Potassium *tert*-butoxide (*t*-BuOK, 97%) was purchased from Alfa Aesar. Divinyl adipate (DVA, >99%) was purchased from TCI. 2,2'-Azobis(2-methylpropionitrile) (AIBN, 98%, Aldrich) was recrystallized from methanol (MeOH) prior to use. Sodium chloride (NaCl) particles were sieved (250-400 µm) and stored in moisture-free conditions. All solvents were used as received: methanol (99.9%), ethanol (99.9%, anhydrous), acetone (99.9%), acetonitrile (ACN, 99.9%), isopropanol (*i*-PrOH, 99.9%), ethyl acetate (AcOEt, 99.9%), tetrahydrofuran (THF, 99.9%), cyclohexane (*c*-Hex, 99.8%), 1,4-dioxane (99.5%), and *n*-heptane (*n*-Hep, 99%) were purchased from Carlo Erba. *n*-Hexane (*n*-Hex ,99%) and benzene (99.8%, anhydrous) were purchased from Thermo scientific and Sigma Aldrich, respectively.

2.2. Preparation of 2-methylene-1,3-dioxepane (MDO)

The cyclic ketene acetal was prepared as previously described by Bailey [29]. 2-chloromethyl-1,3-dioxepane (MDO cyclic precursor) was synthesized by acetal exchange reaction from chloroacetaldehyde dimethyl acetal (50 g, 0.4 mol) in the presence of 1,4-butanediol (36.17 g, 0.4 mol) and Dowex® 50 acidic resin (1.6 g) at 115 °C in a flask equipped with a distillation column. When the expected stoichiometric amount of methanol had been collected from the distillation, the resin was removed by filtration, and the solution was once more distilled under vacuum to afford pure 2-chloromethyl-1,3-dioxepane (yield = 72%). ^{1}H NMR (400 MHz, $CDCl_3$) δ (ppm) 1.65 (m, 4H, -$OCH_2CH_2CH_2CH_2O$-), 3.38 (d, 2H, -CH_2Cl), 3.72 (dd, J = 90.3 Hz, 4H, -OCH_2-), 4.76 (t, 1H, -OC*H*O-). The second step to obtain MDO was the dehydrohalogenation of 2-chloromethyl-1,3-dioxepane. 17.88 g (159.4 mmol) of *t*-BuOK were dissolved in 50 mL of THF at 115 °C in a flask equipped with a water cooler. Then, 12 g (79.7 mmol) of 2-chloromethyl-1,3-dioxepane were added dropwise, and the reaction mixture was allowed to react for 16 h. MDO and THF were separated from the solid components by distillation under vacuum at 130 °C, and finally, MDO was isolated by fractional distillation under vacuum at 80 °C (yield = 69 %). ^{1}H NMR (400 MHz, $CDCl_3$) δ 1.67 (m, 4H, -$OCH_2CH_2CH_2CH_2O$-), 3.34 (s, 2H, CH_2=C), 3.84 (m, 4H, -OCH_2-).

2.3. Preparation of monoporous MDO-based materials

Initially, NaCl templates were prepared by Spark Plasma Sintering (SPS) treatment as previously reported by our group [21]. Briefly, 2.54 g of NaCl sieved particles (250-400 µm) were introduced into a graphite die (10 mm in diameter), heated from room temperature to 100 °C (50 °C/min) while applying 3.3 kN force onto the sample under vacuum. After 20 min, the die was cooled to room temperature at 50 °C/min and the salt templates were recovered (about 10 mm in diameter and 15 mm in height). The NaCl template was introduced into the 1 cm in diameter and 3 cm in height stainless-steel reactor and vacuum was applied to remove air present in the interstices between salt particles to facilitate the penetration of the copolymerization feed. Then, the polymerization mixture containing an MDO/DVA co-monomer mixture (molar ratio of 80/20 mol.%) and AIBN (2 wt.% with respect to the total comonomer quantity) was sonicated until AIBN was completely dissolved and was added into the stainless-steel reactor under static vacuum. The reactor was sealed and placed in an oven at 65 °C for 24 h. After copolymerization, the porogenic 3D template composed of SPS-sintered salt particles was removed by immersing the material in deionized water for 24 h (water was changed 3 times) and finally dried under vacuum at room temperature for 24 h. Materials containing only micropores were prepared following the same procedure by replacing the salt template with a specific volume of *n*-hexane. In this case, MDO/DVA (80/20 mol.%), AIBN (2 wt.% with respect to the total comonomer mass), and *n*-hexane (20/80, 30/70, and 40/60 vol.% comonomer/porogenic solvent) were mixed and the polymerization followed the same conditions as previously described. After copolymerization, the porogenic solvent was removed by Soxhlet extraction using acetone for 16 h and the final materials were dried under vacuum at room temperature for 24 h. In order to identify the monoporous samples, the prefix M is used, thus defining that the sample is monoporous followed by the MDO concentration and then the letter T or S to distinguish between materials polymerized with a salt template or a porogenic solvent, respectively, and followed by the solvent content added to the polymerization mixture. As an example, a material containing 80/20 mol.% MDO/DVA and 30/70 vol.% comonomer/porogenic solvent is labeled as M80S70.

2.4. Preparation of biporous MDO-based materials

The polymerization mixture constituted of MDO/DVA (molar ratio: 80/20, 70/30, and 60/40 mol.%), AIBN (2 wt.% with respect to the total comonomer mass) and *n*-hexane (various comonomers/porogenic solvent volume ratios: 40/60, 30/70, and 20/80 vol.%) was sonicated

until the AIBN was completely dissolved. The NaCl template was introduced into the stainless-steel reactor and vacuum was applied for 10 min after which, the polymerization solution was added. The reactor was sealed and placed in an oven at 65 °C for 24 h. After copolymerization, the porogenic solvent and the NaCl template were removed by immersing the obtained material in deionized water (16 h), acetone (4 h), and again deionized water (4 h). Lastly, the obtained material was dried under vacuum at room temperature for 24 h. In this case, to identify the biporous samples, the prefix Bi is used to define that the sample is biporous followed by the MDO concentration and then by the letter S, ending with the content of solvent. As an example, a material containing 80/20 mol.% MDO/DVA and 20/80 vol.% comonomer/porogenic solvent is labeled as Bi80S80.

2.5. Characterization procedures

2.5.1. Chemical characterization of the P(MDO-*co*-DVA) porous scaffolds

Raman spectra were recorded between 500 and 3500 cm^{-1} using an XPlora One spectrometer from Horiba Jobin Yvon equipped with a laser emitting at 638 nm. The acquisition time was fixed at 1 min.

2.5.2. Porous features of MDO-based materials

The pore size distribution, total intrusion volume, and porosity ratios of the materials were determined by Mercury Intrusion Porosimetry (MIP) using an AutoPore V 9600 porosimeter from Micromeritics based on the Washburn equation where the pore diameter, the applied pressure, the surface tension and the contact angle are related. For the analysis, a 3-cm^3 bulb solid penetrometer was used, and the equilibrium time for low and high pressure was set in 10 seconds. It is important to highlight the appearance of a peak at about 8 µm related to the change from the low-pressure analysis to the high-pressure analysis in all MIP profiles.

SEM investigation of the materials was performed with a MERLIN microscope from Zeiss equipped with SE2 and In Lens detectors using an accelerating tension of 10 kV and a current of 100 pA. Samples were immersed in liquid nitrogen for 5 min, cut into cylinders of approximately 10 mm in diameter by 1 mm in height and coated with a 5 nm layer of platinum/palladium alloy in a Cressington sputter-coater 108 auto with thickness controller MTM-20. The pore sizes were determined using the *ImageJ 1.54d* software.

2.5.3. Mechanical properties

The compressive mechanical properties of the materials were investigated in dry state at room temperature in a universal testing machine INSTRON 5965 equipped with a 100 N load cell.

The studied materials have an approximate size of 10 mm in diameter and 15 mm in height. The compression rate was set at 1 mm/min, and the maximum displacement at 70%. The compressive modulus is the relation between the tensile stress and the tensile strain. It is obtained by fitting a straight line over the linear part of the stress-strain curve (between 0 and 10% strain). **Equation 1** shows the representation of the compressive modulus:

$$Compressive\ modulus(MPa) = \frac{\Delta\ stress\ (MPa)}{\Delta\ strain\ (\%)} \times 100 \quad \textbf{(Equation 1)}$$

2.5.4. Water uptake

Biporous and monoporous dry materials were immersed in 5 mL of deionized water for 47 days at room temperature. After different periods of time, materials were taken out of the vial, and after elimination of the excess of water on the surface with paper, they were weighed. The measurements were conducted in quadruplicate, and the averages were used for the analysis. The water uptake was calculated according to **Equation 2**:

$$Water\ uptake\ (\%) = \frac{W_w - W_d}{W_d} \times 100 \quad \textbf{(Equation 2)}$$

where W_w is the weight of the wet material and W_d is the weight of the dry material.

The adsorption mechanism was investigated by fitting the data to the intraparticle diffusion, thanks to pseudo-first order and pseudo-second order kinetic models.

The intraparticle diffusion model was given by **Equation 3** [30,31] :

$$q_t = k_{id} t^{0.5} + C \quad \textbf{(Equation 3)}$$

where q_t is the adsorbed water mass per unit time at a specific time and k_{id} is the intraparticle diffusion rate constant ($mg.g^{-1}.h^{-½}$). The values of k_{id} and C could be obtained from the linearization of q_t *vs.* $t^{1/2}$, where the slope represents k_{id} and C is the intercept.

The pseudo-first order kinetic model was given by **Equation 4** [30,32] :

$$\mathrm{Ln}(q_e - q_t) = -k_1 t + \ln\,(q_e) \quad \textbf{(Equation 4)}$$

where q_t is the adsorbed water at a specific time, q_e is the adsorbed water at equilibrium, and k_1 is the pseudo-first order rate constant (h^{-1}). In order to obtain the model parameters, $\mathrm{Ln}(q_e - q_t)$ *vs.* t was plotted, and from the linearization, k_1 and q_e are related to the slope and the intercept, respectively.

The pseudo-second order model was expressed by **Equation 5** [32,33] :

$$\frac{t}{q_t} = \frac{1}{k_2 q_e^2} + \frac{t}{q_e} \quad \textbf{(Equation 5)}$$

where k_2 is the pseudo-second order rate constant ($g.mg^{-1}.h^{-1}$), q_t and q_e were previously described. Model parameters were obtained by plotting t/q_t *vs.* t in which q_e and k_2 are related to the slope and the intercept, respectively.

2.5.5. Degradability

Bi80S80 biporous MDO-based materials prepared using an MDO/DVA molar ratio equal to 80/20 were placed in glass vials under vacuum at room temperature for 10 min to remove air from the porosity. Firstly, 3.33 mL of ethanol were injected under static vacuum to fill the pores of the material for 10 min, then 5 mL of 0.1 M phosphate-buffered saline (PBS, thermo scientific) pH 7.4 or 5 mL of a 0.1 wt.% NaOH aqueous solution were added. The samples were placed in an oven (Heratherm OMH60) at 37 °C. Regularly the samples were washed with deionized water, dried under vacuum, and weighed. Each time, the ethanol-PBS mixed solution was replaced following the same procedure. For achieving accelerated conditions, the materials were placed in a 60/40 vol.% NaOH aqueous solution (1, 3 or 5 wt.%)/EtOH mixture. Depending on the degradation rate, the samples were recovered, washed with deionized water, dried under vacuum, and weighed at different time intervals. Each time, the 3 and 5 wt.% NaOH hydrolysis solutions were replaced, while those containing 0.1 and 1 wt.% NaOH were replaced every week.

Finally, ultrafast degradation conditions were tested by immersing the Bi80S80 biporous MDO-based materials in 10 mL MeOH in which 500 mg of NaOH were previously dissolved.

3. Results and discussion

3.1. Preparation of monoporous and biporous materials

An effective strategy to fabricate bimodal porous polymeric networks relies on the double porogen templating approach (**Figure 1a**), as previously reported by our group [20–22,34,35] in which the macroporosity is generated by the leaching of an inorganic matrix and the lower porosity level is afforded by polymerization-induced phase separation. The total porosity and pore interconnectivity strongly depend on particle size, shape, and arrangement in the macroporogen template as well as the solvent nature and its proportion in the polymerization mixture. Based on these important parameters, the double porogen templating approach permits to produce materials with hierarchically controlled pore size and pore interconnectivity.

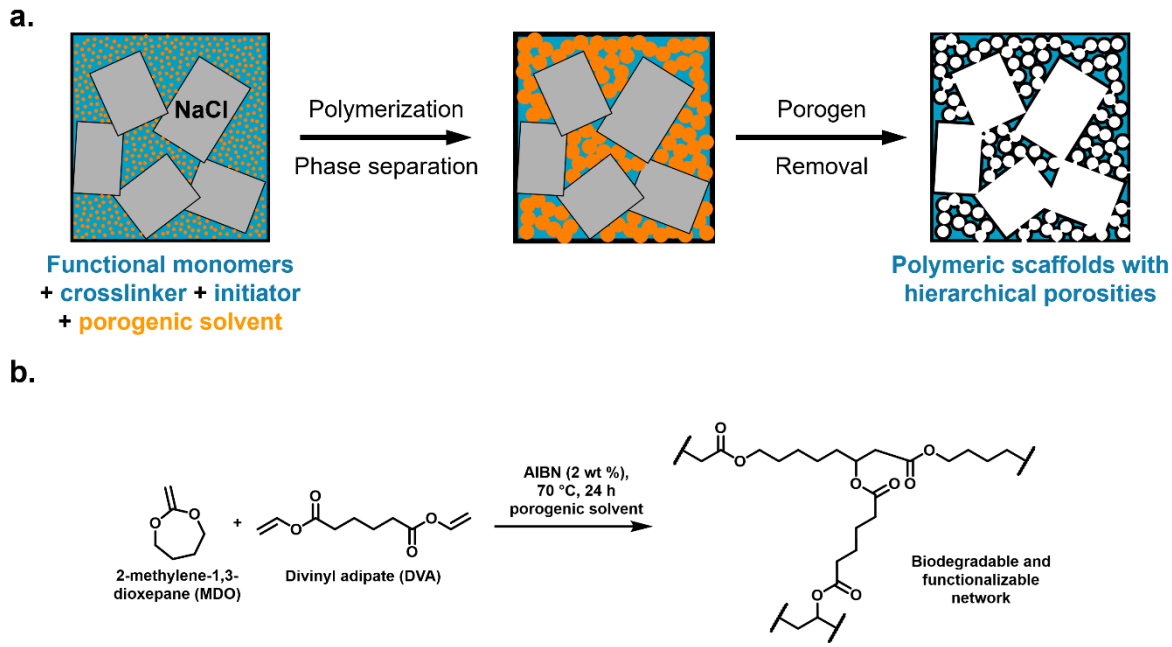

Figure 1. (a) Schematic representation of the double porogen templating approach using sintered NaCl particles as macroporogens and a porogenic solvent. (b) General reaction for the preparation of porous networks through free-radical ring-opening copolymerization of 2-methylene-1,3-dioxepane with divinyl adipate as a crosslinker in the presence of a porogenic solvent.

Generally, when a high ratio of CKA to vinyl monomers, such as (meth)acrylates and styrene, is used, the global CKA conversion decreases with its poor incorporation into the copolymer backbone [36]. The latter limitation could be related to the surprisingly low reactivity ratio of MDO even though a strong nucleophilicity from the acetal oxygens and the C=C bond could promote the polymerization with electrophilic radicals, such as those generated by acrylate derivatives [36,37]. Thus, to prepare a homogeneous MDO-based network, the selection of a comonomer with similar reactivity becomes crucial. In a general manner, CKA monomers present a low incorporation ratio when copolymerized with a lot of monomers such as styrenics, acrylates and methacrylates, excepted for vinyl acetate (VAc) [36]. Several studies have been previously performed to estimate the reactivity ratios between different CKA and VAc by different methods. Reactivity ratio (r_{CKA} and r_{VAc}) values in the order of 10^{-1} and 10^{1} for CKA and VAc have been found, respectively. [38], [39], [40], [41], [36] In one of these studies, Agarwal *et al.* [39] have shown the successful copolymerization of MDO and VAc with yield up to 80% by (c)rROP due to their closer reactivity ratios (r_{MDO} = 0.47 and r_{VAc} = 1.53), which allows the introduction of ester functionalities into the copolymer backbone. In this regard, divinyl adipate (DVA) possess two polymerizable functions similar to MDO and VAc, thus making it a promising cross-linking agent of choice due to its well-known

biocompatibility and similar reactivity to that of MDO. Indeed, reactivity ratios in the same order of magnitude were observed for DVA (r_{DVA} = 0.034 and r_{St} = 20.6) [42] and MDO (r_{MDO} = 0.021 and r_{St} = 22.6) [43] when copolymerizing them with styrene.

In order to produce a biodegradable and biocompatible polymeric network, MDO was chosen as a suitable monomer because it has been used to introduce ester functions into the polymeric chains and improve the degradability of the applied materials. In addition, by free-radical ring-opening polymerization, the resulting structure is similar to PCL, which is mostly used in biomedical applications (**Figure 1b**) [23]. The chemical nature of the as-obtained scaffolds was assessed by Raman spectroscopy (**Figure S1**, ESI). The spectrum of the network notably highlighted the presence of C=O characteristic ester band at ~1750 cm^{-1}. Interestingly, no band corresponding to C=C double bond was observed, thus suggesting total consumption of ketene acetal and vinyl ester functionalities through free-radical copolymerization. Generally, MDO is used in low quantities in copolymerization feeds to increase the degradability of diverse (co)polymers, while DVA, to the best of our knowledge, has not been used to create polymeric networks. Therefore, as a starting point of our investigation, the copolymerization of both comonomers was studied. The effect of varying molar compositions, solvent ratios, and the use of macroporogens instead of porogenic solvent were studied with a particular focus on the mechanical properties of resulting materials. Finally, their degree of degradation and water adsorption was investigated.

3.2. Porous features of MDO-based materials

It has been demonstrated that the use of NaCl particles is an effective strategy to produce a macroporous matrix. The interconnectivity of the structure highly depends on the packing degree of the inorganic template: for instance, a non-sintered template leads to isolated macropores with different shapes and reduced specific surface area [20], while a sintered template and especially that made by SPS presents a well-defined morphology with interconnected pores and larger specific surface area [21]. Biporous polymeric networks Bi80S80 were obtained after complete removal of the NaCl template and the porogenic solvent. As observed by SEM (**Figure 2a,b,c**), MDO/DVA scaffolds displayed a bimodal porosity. The presence of homogeneous macropores with size around 200 µm related to the NaCl template imprint is in good agreement with the size of the salt particles used to produce the template, while smaller pores with size of about 1.8 µm were due to the porogenic solvent removal. The size of the smaller pores was similar to those obtained in the copolymerization of porous hydroxyethyl methacrylate (HEMA) and ethylene dimethacrylate (EDMA) when *n*-

hexane was used as a porogenic solvent [44]. Moreover, it has been demonstrated that depending on the solvent polarity compared to that of network components, the porogenic solvent may lead to different pore sizes with larger pores (~1 µm) obtained from non-polar solvents and smaller pores (~100-300 nm) expected from polar solvents [21]. For the sake of comparison, **Figure 2d,e** presents the SEM image of monoporous MDO-based analogues obtained using the same MDO/DVA molar ratio using only the NaCl template as porogen (M80T). **Figure 2f,g** shows the SEM micrographs of other monoporous counterpart obtained by using *n*-hexane as the porogenic solvent (M80S80). The compact globular morphology of the lower scale porosity could be explained as follows. The polymerization mixture was composed of comonomers, initiator, and the porogenic solvent. The free radicals generated from AIBN triggered the copolymerization process. Due to crosslinking of the copolymer chains, they became insoluble and precipitated as particles at a more or less early stage, during the copolymerization process depending on their compatibility with the porogenic solvent. These particles enlarged as the surrounding chains grew, thus forming a globular cluster which shape was related to the tension at the liquid-solid interface and to the affinity for the organic phase. The clusters formed continuously and dispersed in the media, leading to the formation of an interconnected matrix. The space between these large clusters created voids which total volume is similar to that of the porogenic solvent initially present in the polymerization feed, as already reported elsewhere. [21]. The size of the globular structures and voids depended on key factors, such as the polymerization temperature, initiator concentration, and solvent characteristics.

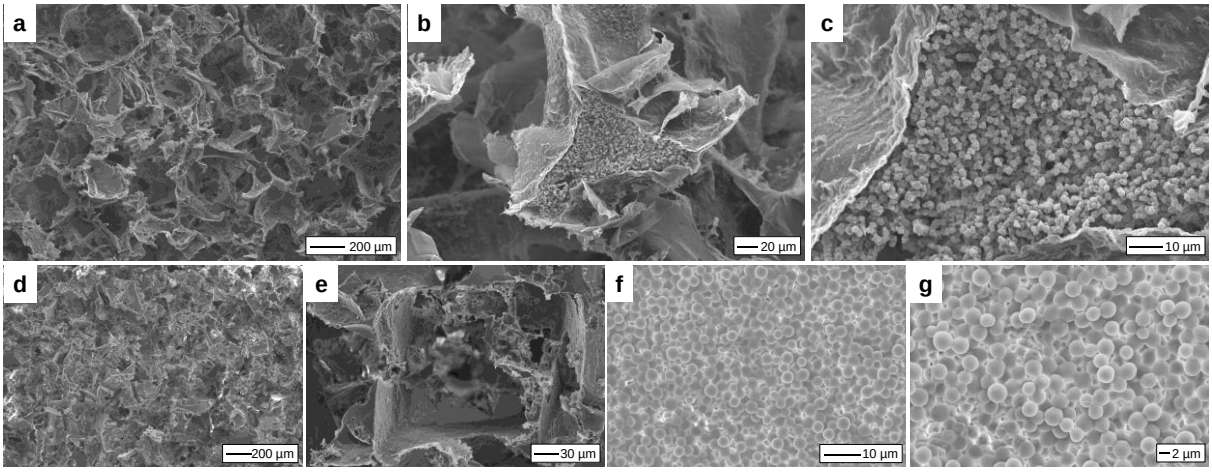

Figure 2. SEM images of MDO-based networks: (a,b,c) Biporous scaffold (80/20 mol.% MDO/DVA and 80 vol.% *n*-hexane with respect to the comonomers), (d,e) monoporous analogue using NaCl template, (f, g) monoporous analogue using *n*-hexane.

While the upper porosity level resulting from salt-sintered templates is determined by the NaCl particle size and the sintering method used [21], the lower porosity level is obtained independently by phase separation during the polymerization in the presence of a porogenic solvent. It thus presents an interesting area of study due to some tunability inherent to different experimental parameters. In this case, the pore size distribution is governed by various key parameters, including the nature and volume of the porogenic solvent used, for instance. The possibility to finely tune the porosity obtained from the syneresis mechanism during the copolymerization was thus investigated as it clearly permitted to control the porous features of the resulting materials, which may hold relevance for further biomedical applications. Different common organic solvents were assessed as possible porogens. Based on their solubility parameters, methanol (MeOH), ethanol (EtOH), acetonitrile (ACN), isopropanol (*i*-PrOH), benzene, tetrahydrofuran (THF), ethyl acetate (AcOEt), cyclohexane (*c*-Hex), dioxane, *n*-heptane (*n*-Hep), and *n*-hexane (*n*-Hex) were used. Even though CKAs exhibit relative instability and are prone to alcoholysis in the presence of a large excess of alcohol [45], resulting in the production of undesirable by-products that impede further polymerization reactions and have an autocatalytic effect towards self-degradation [46], MeOH and EtOH were used for the sake of comparison as the solvent properties are crucial regarding the porous features of the resulting materials [21]. **Figure 3a** shows the MIP profiles of monoporous materials constituted of 80/20 mol.% MDO/DVA after copolymerization in the presence of 80 vol.% of the tested porogenic solvent and further removal. The corresponding data extracted from the MIP analyses are summarized in **Table 1**. Among all investigated solvents, only the non-polar ones (*c*-hexane, *n*-heptane, and *n*-hexane), *i.e.* displaying the lowest solubility parameters, allowed for obtaining a polymer matrix with a desired porosity, namely an average pore size of around 1 µm. The use of such solvents resulted in a pore size distribution in the 1-2 µm range, a porosity ratio comprised between 68 and 72 % along with an intrusion volume around 1.9-2.4 mL/g (MIP profiles and porous features of the biporous counterparts are shown in **Figure S2** and **Table S1**, ESI). Meanwhile, using MeOH and EtOH as the porogenic solvents gave higher porosity ratios (83-84 %) and intrusion volumes (5.3-5.6 mL/g), but unfortunately too large pore size (9.5 µm) with MeOH. It is worth mentioning that the lower pore size (2 µm) of the scaffold obtained from EtOH as the porogenic solvent could be likely due to the compression of the structure during the high pressure analysis of MIP giving an under-estimated value of the pore size [47]. The Flory-Huggins interaction parameter (χ) allows for studying the interaction between the porogenic solvent and the copolymers in the system [48,49]. It could be related to the

solubility parameter by the Van Laar-Hildebrand equation [50] using Van Krevelen's group molar attraction contributions [51]. The relation of the interaction parameter as function of the molar concentration of MDO could be observed in **Figure 3b**. Theoretically, an increase in χ was observed when increasing the MDO concentration in the case of a poor solvent. On the contrary, a decrease of χ could be observed when increasing MDO concentration in the case of a good solvent for the system [51]. Thus, solvents such as *c*-hexane, *n*-heptane, and *n*-hexane would be suitable for the hydrophobic monomers mixing. As the polymerization occurred, the ring-opened structure of MDO reacted with the vinyl ending groups of DVA leading towards a rather hydrophobic copolymer containing ester functionalities that would precipitate lately during the copolymerization process. The non-polar solvents were thus involved in the formation of smaller sized pores. On the contrary, when methanol or ethanol were used as porogenic solvents, they were expelled earlier during the copolymerization process, thus resulting in the formation of larger sized pores. It is worth mentioning that copolymerizing MDO and DVA in the presence of MeOH/EtOH as the porogenic solvent resulted in polymeric scaffolds with poor mechanical properties. The brittleness of such monoporous scaffolds notably did not allow them to be used afterwards for the preparation of biporous polymeric structures.

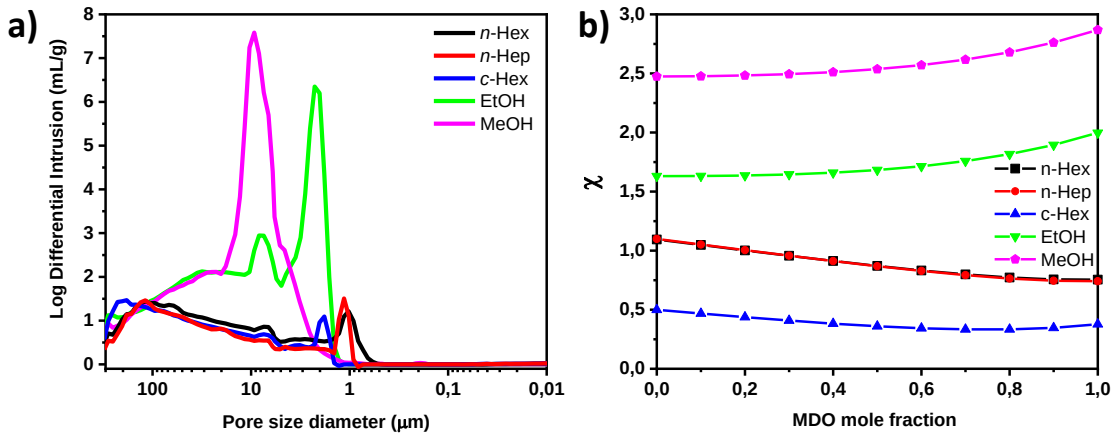

Figure 3. (a) MIP profiles of monoporous MDO-based networks obtained using different porogenic solvents. (b) Evolution of the Flory-Huggins interaction parameter χ as a function of MDO mole fraction.

Table 1. Porous features of monoporous MDO-based networks prepared with various porogenic solvents.

Porogenic solvent	Porosity ratio[a] (%)	Average pore size[a] (µm)	Total intrusion volume[a] (mL/g)	δ[b] (MPa$^{1/2}$)
n-Hexane	72	1.0	2.4	14.9
n-Heptane	68	1.1	1.9	15.1

c-Hexane	69	1.8	2.0	16.8
EtOH	84	2.2	5.6	26.0
MeOH	84	9.5	5.3	29.7

[a] Values as determined by MIP.
[b] Solubility parameters cited from literature [51]

The variation of the porogenic solvent content in the initial copolymerization feed was then varied from 80 to 60% vol.%, and the MIP profiles of resulting monoporous materials were analyzed. They are displayed in **Figure 4a**, and the porous features data are summarized in **Table 2** (MIP profiles and porous features of their biporous counterparts are shown in **Figure S3** and **Table S2**, ESI). It could be easily shown that the lower the *n*-hexane content, the larger the pore size. The pore size of networks containing 70 and 60 vol.% of *n*-hexane was found to be equal to 1.8 and 3.6 µm, respectively, with an almost linear decrease in the porosity ratio and in the intruded mercury volume. As previously explained, closed pores could be obtained as a result of the random formation of the voids causing a decrease in the porosity ratio.

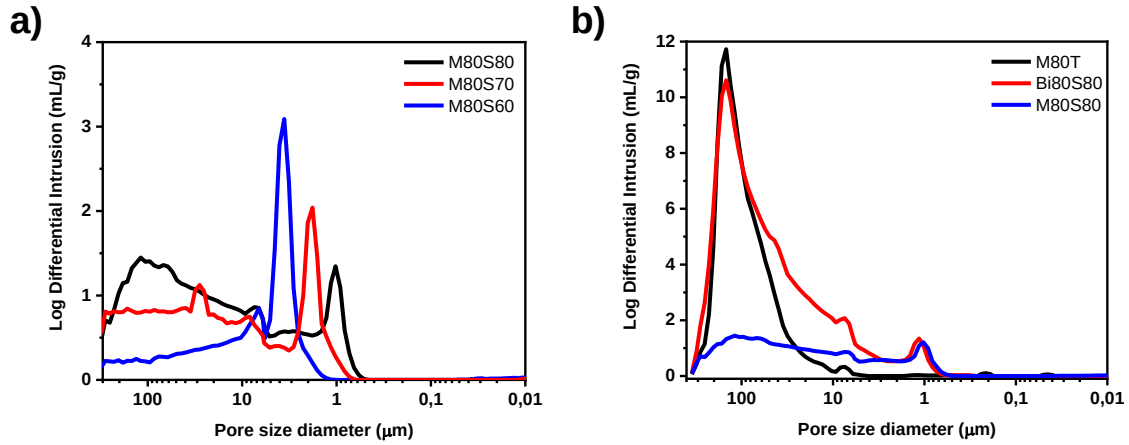

Figure 4. MIP profiles of (a) monoporous MDO-based networks prepared with various contents of *n*-hexane as a porogenic solvent and (b) typical monoporous (M80T and M80S80) and biporous (Bi80S80) MDO-based materials.

Table 2. Porous features of monoporous MDO-based networks prepared with various contents of *n*-hexane as a porogenic solvent.

Sample	**Porosity ratio[a] (%)**	**Average pore size[a] (µm)**	**Total intrusion volume[a] (mL.g^{-1})**
M80S80	72	1.0	2.4
M80S70	62	1.8	1.6
M80S60	54	3.6	1.0

[a] Values as determined by MIP.

MIP profiles of typical MDO-based materials depending on the used porogen are shown in **Figure 4b**, while porosity ratio, pore size, and total intrusion volume values are summarized in **Table 3**. Monoporous materials M80T and M80S80 presented a unimodal pore size distribution with pore sizes centered around 148 µm and 1 µm, respectively, depending on the nature of the corresponding porogen. The biporous material Bi80S80 displayed a bimodal porous distribution profile constituted of large pores arising from the removal of the salt template with an average size centered around 150 µm and smaller pores arising from the extraction of the porogenic solvent of around 1.1 µm; such pore sizes were in good agreement with those obtained for their monoporous counterparts. Furthermore, the porosity ratio of the biporous material as well as the total intrusion volume (89 % and 9.7 $mL.g^{-1}$) were found to be higher than those of the monoporous materials obtained with the salt template (82 % and 5.3 $mL.g^{-1}$) and the porogenic solvent (72 % and 2.4 $mL.g^{-1}$), providing the evidence of a good pore interconnectivity. The porosity obtained from the monoporous sample prepared with the porogenic solvent is lower than that expected for 80 vol.% *n*-hexane used and the small intrusion volume could be explained by the polymerization process and the random generation of the voids that could lead to their partial or complete blockage, thus preventing the mercury from reaching the small cavities [47,52]. Biporous and monoporous MDO-based materials with a variation on crosslinking agent concentration were also investigated (MIP profiles shown in **Figure S4** and **Figure S5**; porous features listed in **Table S3** and **Table S4**, ESI). As already observed in previous studies, the increase in crosslinker content in the polymerization feed allows for obtaining pores with a higher average size. In this study, increasing DVA content from 20 to 40% allowed for increasing average pore size from 1 to 2.5 µm and from 1.1. to 2.7 µm in monoporous and biporous polymers, respectively.

Table 3. Porous features of mono-and biporous MDO-based materials.

Sample	Porosity ratio[a] (%)	Average pore sizes[a] (µm)	Total intrusion volume[a] ($mL.g^{-1}$)
Bi80S80	89	150 and 1.1	9.7
M80T	82	148	5.3
M80S80	72	1.0	2.4

[a] Values as determined by MIP.

3.3. Mechanical properties of MDO-based materials

Producing scaffolds with mechanical properties suitable for the target tissue environment is of paramount significance in tissue engineering applications. Upon implantation, a polymer scaffold should support interactions with cells and new tissue formation. To this purpose, it

must maintain its mechanical integrity throughout the overall process until complete regeneration of the damaged tissue [5]. Even though the increase in porosity, pore interconnectivity, and pore size is beneficial to cell ingrowth of the scaffold and vascularization of engineered tissues, it could compromise the mechanical stability of the material [7]. In order to investigate the applicability of our as-prepared model materials to tissue engineering, compressibility tests were performed with mono- and biporous MDO-based polymeric networks. **Figure 5** shows the compressive stress-strain curves of M80T (using only NaCl template) and Bi80S80 scaffolds. It allows for the determination of Young's modulus, *E*, the yield stress at 10% of deformation, σ_{10}, and the end point of the deformation plateau, σ_{SP}, as summarized in **Table 4**. We could observe three different regimes in the graph: a linear behavior at small strain (<10%) where Young's modulus could be calculated, followed by a stage where deformation took place which was characterized by a small increase in stress but large elongation (~50%), and the last zone related to the complete compression of the structure where the stress increased rapidly with moderate deformation. The MDO-based material presenting a bimodal porosity showed an elastic modulus *E* equal to 32.7 ± 2.5 kPa with a compressive strength at 10% strain of 2.5 kPa. These values were smaller than those associated with that the monoporous analogue containing only macropores (M80T): E = 43 ± 5.2 kPa and σ_{10} = 4.5 kPa. In addition, the biporous structure showed an elongation of 56% and 20 kPa at the end of the deformation plateau, before the stage of complete compression, while the monoporous analogue had an elongation of 51 % and 24.5 kPa at the end of the deformation plateau. The decrease in Young's modulus was probably related to the higher porosity ratio of the biporous scaffolds compared to the monoporous ones (**Table 4**). This result was in good agreement with other results obtained for porous poly(L-lactide-*co*-D,L-lactide) scaffolds [53], where a decrease of the elastic modulus from 168 MPa to 43 MPa was observed when the porosity ratio increased from 58 % to 80 %. It is worth noticing that monoporous scaffolds obtained only with a porogenic solvent could not be tested regarding mechanical properties due to their brittleness.

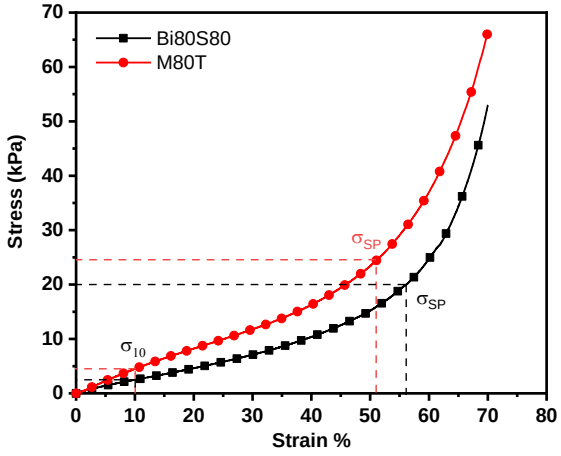

Figure 5. Compressive stress-strain curves of monoporous and biporous MDO-based networks.

The effect of the solvent content on the biporous MDO-based materials was also investigated by adjusting the volume percentage of *n*-hexane in the polymerization feed. Bi80S80, Bi80S70 and Bi80S60 were examined in terms of their compressive properties (**Figure 6a**); the values of E, σ_{10}, and σ_{SP}, are also summarized in **Table 4**. Surprisingly, the latter measured parameters decreased as the volume ratio of porogenic solvent was reduced. For instance, the material containing 60 vol.% of *n*-hexane, *i.e.* Bi80S60, presented an elastic modulus of 14.4 ± 2.3 kPa, while the material Bi80S70 containing 70 vol% showed a value of 32.0 ± 4.1 kPa and the reference scaffold prepared using 80 vol% *n*-hexane, *i.e.* Bi80S80, displayed a value of 32.7 ± 2.5 kPa: a drastic decrease of the elastic modulus of ~56% was thus observed upon a 20 % reduction of the amount of porogenic solvent. The yield stress at 10% strain for materials containing 60 and 70 vol.% of *n*-hexane was found to be equal to 1.1 ± 0.1 and 2.0 ± 0.4 kPa, which represented a significant reduction of ~56 and ~20% when compared to the scaffold prepared with 80 vol.% *n*-hexane (2.5 ± 0.6 kPa). Furthermore, the stress measured at the end point of the deformation plateau was equal to 6.6 ± 1.1 and 9.9 ± 0.5 kPa for scaffolds containing 60 and 70 vol.% of porogenic solvent, representing a dramatic reduction of 67 and 50 % compared to the material prepared with 80 vol% *n*-hexane. These results were not in agreement with those previously obtained [7,53] resulting from a relation existing between the porosity and the compressive properties. Nevertheless, we assume that this unique behavior could be related to the solvent interactions in the system in addition to the low activity of the monomers as a polymeric network could exhibit different structures and properties depending

on the concentration of crosslinking agent used and on the solvating ability of the porogenic solvent [54].

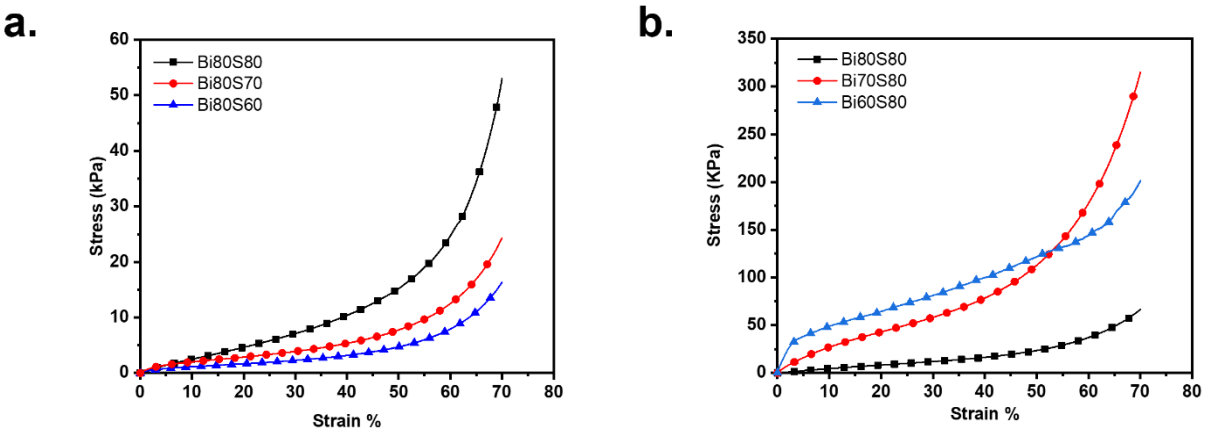

Figure 6. Compressive stress-strain curves of biporous MDO-based materials obtained (a) using various contents of *n*-hexane as a porogenic solvent (60, 70, and 80 vol.%) or (b) using 20, 30, and 40 mol.% DVA as a crosslinker.

As the concentration of the crosslinking agent is a key parameter during the formation of the polymeric network, its effect was investigated by varying the molar concentration of DVA in the polymerization feed (MDO/DVA molar ratio: 80/20, 70/30, and 60/40 mol.%) while maintaining constant the solvent content to 80 vol.% of *n*-hexane, as it showed an elastic behavior with better compressive features. **Figure 6b** exhibits the stress-strain curves of the latter materials with different crosslinker concentrations, and the data obtained from the graphs are gathered in **Table 4**. It could be observed that the resistance against a compressive load increased as the concentration of crosslinking agent increased. Setting the molar concentration of DVA to 30 mol.% resulted in an increase in the elastic modulus of 767 % (283.7 ± 37.8 kPa), while a 40 mol.% DVA concentration allowed for a 3200% increase in the Young´s modulus (1085.3 ± 92.3 kPa), as compared to the material containing 20 mol.% DVA. On the other hand, the stress at 10% strain was equal to 26 ± 7.3 kPa and 48 ± 9.1 kPa representing an increase of 940 % and 1820 %, respectively for materials constituted of 30 and 40 mol.% DVA, as compared to the measured value for the material containing 20 mol.% DVA. The yield stress at the end point of the deformation plateau for the 30 mol.% DVA scaffold was equal to 121 kPa (six times higher than that measured for 20 mol.% DVA), while the analysis for the scaffold containing 40 mol.% DVA could not be performed properly due to sample breakage at ~50 % strain, where the maximum stress was equal to 124 kPa. The latter results could be due to the mechanism of formation of the polymeric network in which an increase in crosslinker concentration, while keeping constant the solvent volume, might

lead to a rapid phase separation and generation of small nuclei that would keep growing and reacting with each other through the vinyl functions and the radical centers in the mixture, thus affecting the pore size distribution and resulting in an increase of Young's modulus, reducing the elasticity and increasing the material resistance to compression.[54,55].

Table 4. Compressive mechanical properties of MDO-based materials.

Sample	MDO/DVA molar ratio (mol.%)	Porogenic solvent (vol.%)	E^a (kPa)	$\sigma_{10}{}^b$ (kPa)	$\sigma_{SP}{}^c$ (kPa)
M80T	80/20	-	43.0 ± 5.2	4.5 ± 0.5	24.5 ± 2.7
Bi80S80	80/20	80	32.7 ± 2.5	2.5 ± 0.6	20.0 ± 1.4
Bi80S70	80/20	70	32.0 ± 4.1	2.0 ± 0.4	9.9 ± 0.5
Bi80S60	80/20	60	14.4 ± 2.3	1.1 ± 0.1	6.6 ± 1.1
Bi70S80	70/30	80	283.7 ± 37.8	26.0 ± 7.3	122.0 ± 22.7
Bi60S80	60/40	80	1085.3 ± 92.3	48.0 ± 9.1	124.0 ± 34.2*

[a] *E:* Young's modulus.
[b] σ_{10}: Yield stress at 10% of deformation.
[c] σ_{SP}: Stress at the end point of the deformation plateau.
* Stress at break.

3.4. Water uptake of MDO-based networks

In order to prepare a suitable material for tissue engineering, it is necessary to investigate its capability of up taking physiological fluids, allowing cell suspensions to travel though the scaffold while transferring oxygen, nutrients, and metabolites. In addition, the ability of the scaffold to adsorb water becomes relevant because hydrolysis is the principal mechanism of polymeric scaffold degradation in the human body, which can affect the integrity of the material depending on the degradation rate. Therefore, water uptake experiments were conducted on typical mono- and biporous materials prepared from MDO (**Figure 7a**). It could be observed that the presence of a bimodal porosity greatly improved the water uptake ability (2306 ± 304 %) in a synergistic fashion when compared to monoporous materials constituted of large macropores (754 ± 15 % using only the sintered 3D NaCl template) or smaller pores (268 ± 37 % using only porogenic solvent). Moreover, it could be seen that monoporous materials reached an adsorption equilibrium faster (16 days for M80T and 14 days for M80S80) as compared to the biporous analogue (27 days), which coud be possibly attributed to the ease of water transfer into the different interconnected pore levels. Water absorption mechanism was theoretically assessed by intraparticle diffusion, pseudo-first order, and pseudo-second order kinetic models. [30–33] The results are plotted in **Figure 7b,c,d** for biporous, monoporous with large macropores and smaller pores, respectively, and the corresponding kinetic parameters are listed in **Table 5**.

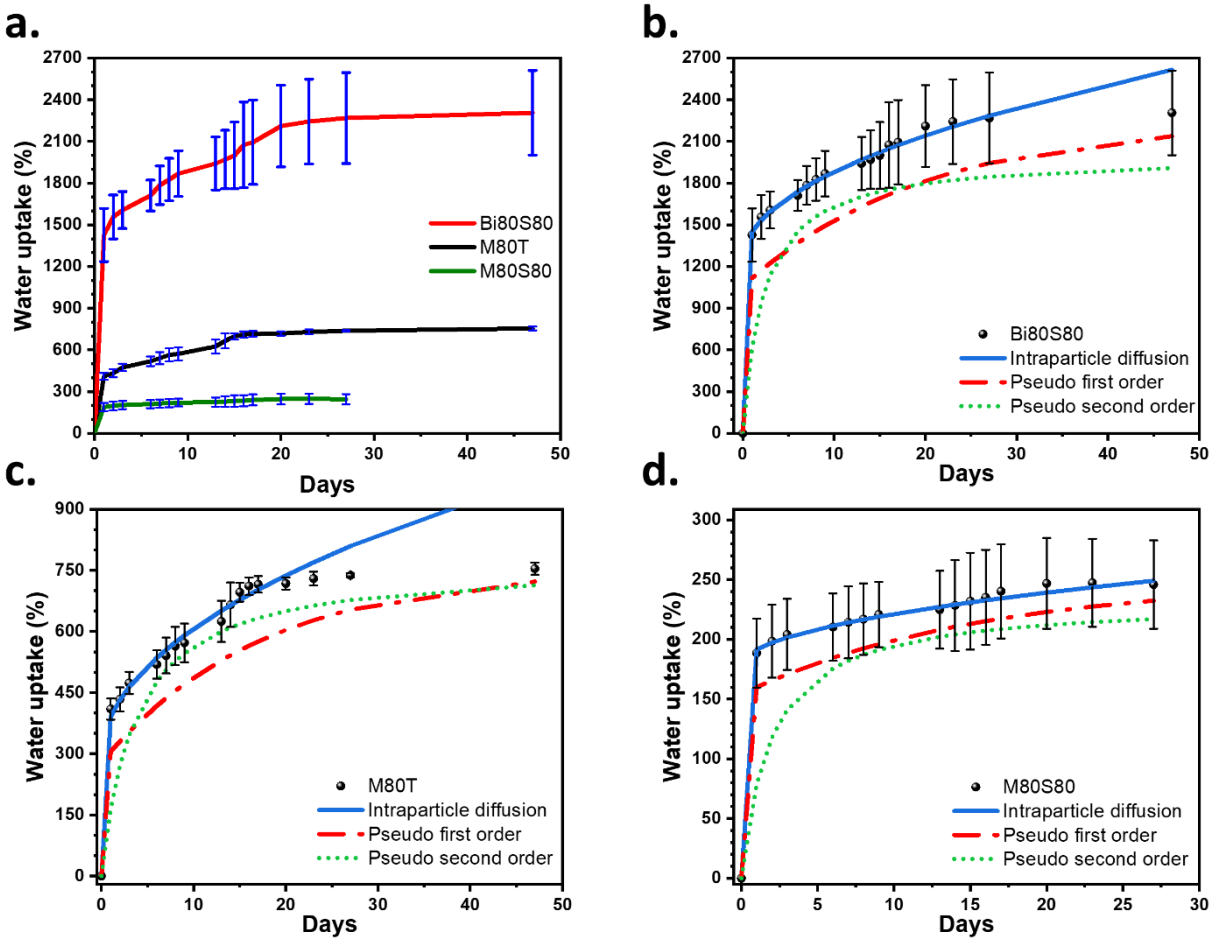

Figure 7. (a) Evolution of water uptake as a function of time for monoporous and corresponding biporous materials depending on the porogens used. Kinetic models theoretically plotted for (b) biporous, or monoporous materials using (c) NaCl template and (d) *n*-hexane as porogens.

Table 5. Theoretically determined characteristic values associated with water uptake kinetic models for mono- and biporous MDO-based networks.

Sample	Intraparticle diffusion		Pseudo-first order			Pseudo-second order		
	k_{id} [a] ($mg.g^{-1}.h^{-1/2}$)	R^2	k_1 [b] ($10^{-3}.h^{-1}$)	q_e [c] ($mg.g^{-1}$)	R^2	k_2 [d] ($g.mg^{-1}.h^{-1}$)	q_e [c] ($mg.g^{-1}$)	R^2
Bi80S80	40.7	0.988	2.1	1192	0.932	$9.22.10^{-6}$	2000	0.943
M80T	20.4	0.976	2.4	475	0.918	$1.48.10^{-5}$	769	0.919
M80S80	2.8	0.982	2.7	95	0.841	$9.21.10^{-5}$	233	0.946

[a] k_{id}: intraparticle diffusion rate constant.
[b] k_1: pseudo-first order rate constant.
[c] q_e: Mass of adsorbed water at equilibrium.
[d] k_2: pseudo-second order rate constant.

Pseudo-first order model varied on all analyzed systems as the calculated adsorbed water at equilibrium (q_e) differed from the experimental values as along with a poor correlation coefficient (R^2). On the other hand, from the pseudo-second order model, q_e values closer to the experimental data were obtained (variation of 12, 5 and 7 % for biporous, M80T and

M80S80 materials, respectively) and the correlation coefficient was above 0.91 for the three materials; still, the profile obtained from this model differed from the experimental behavior. Furthermore, the best fitting model was intraparticle diffusion, especially over 20 days where correlation coefficient was above 0.97 for all materials indicating that the internal diffusion through the pores was the predominating process, showing a strong initial adsorption. The intraparticle diffusion rate constant (k_{id}) was found to be equal to 40.6 $mg.g^{-1}.h^{-1/2}$ for the materials presenting a bimodal porosity, while values of 20.3 and 2.8 $mg.g^{-1}.h^{-1/2}$ were obtained for M80T and M80S80 macroporous and microporous materials, respectively, thus highlighting a great synergetic effect of the bimodal porosity towards the water adsorption ability. Interestingly, the materials were observed to keep the shape of the initial dry state, even the Bi80S80 which displayed a water uptake of 2300%, thus demonstrating that negligible swelling took place during the absorption process, probably due to the relatively high crosslink density of networks under investigation (**Figure S6**, ESI).

3.5. Degradability of MDO-based networks

Degradation rates of materials designed for tissue engineering is a key parameter in their success, as a fast degradation could compromise the mechanical stability of the scaffolds, while a slow degradation could inhibit the adequate regeneration of tissue in the wound area. Degradability of biporous MDO-based materials was investigated under two contrasted experimental conditions, namely accelerated hydrolytic degradation (alkaline media) and under phosphate buffer solution (mild hydrolytic conditions). Time dependence of mass loss is displayed in **Figure 8**.

Upon immersion of the biporous materials in PBS at pH 7.4, no mass loss was observed before 100 h, and it was not until 200 h that a small degradation (0.7 wt.%) could be measured. The maximum degradation obtained in PBS was 5 wt.% after 2400 h. Therefore, harsher alkaline media with increasing concentrations of NaOH from 0.025 to 1.25 M were prepared and tested. As expected, an increase in NaOH concentration, namely the pH of the immersion medium, led to faster degradation rates. Using 5 wt.% NaOH solution degradation medium resulted in a fast degradation of the biporous scaffolds. 94 wt.% of the initial mass of the crosslinked matrix was degraded within 7 h, while 88 wt.% was observed for 3 wt.% concentration within 27 h and a much slower degradation of 97 wt. % for 1 wt.% solution was obtained within 840 h. Degradation of the materials under 0.1 wt.% of NaOH had a similar behavior as in PBS in which only 5 % mass reduction was observed after 2400 h. Interestingly, plots from 1-5 wt.% NaOH showed a slow degradation rate at the beginning up

to 5 wt.% followed by a dramatic mass loss. The crosslinked polymeric network exhibited a bulk degradation due to the cleavage of the ester bonds in the matrix, leaving carboxyl and hydroxyl end groups that relaxed the network allowing for further reactions between the medium and the reactive ester groups. Therefore, the concentration of soluble small oligomer fragments increased, while the concentration of crosslinked ester units decreased over time, causing the exponential loss of mass. In order to quantify the different degradation rates, the kinetics for catalyzed hydrolysis were evaluated, as reported elsewhere [56], and corresponding kinetic parameters are summarized in **Table 6**. The degradation rate *k* in a 5 wt.% NaOH medium was found to be equal to 0.657 h^{-1}, *i.e.* 5.6 times higher than that obtained in a 3 wt.% NaOH aqueous solution, 144 times higher than that obtained for a 1 wt.% NaOH, and ~36 000 times greater than that obtained for the medium with the lowest NaOH concentration (0.1 wt.%) and for PBS buffer solution after 2400 h of degradation. For the sake of comparison, the same degradation assays were achieved on bulk nonporous MDO-based materials to highlight the influence of the porosity and more particularly of the specific surface area of the as-prepared polymeric scaffolds. As expected, much slower degradation kinetics were observed for nonporous materials, as highlighted on **Figure S7 (ESI)**. A ~7% weight loss was measured after 12 h for bulk nonporous materials while Bi80S80 biporous ones showed a 90% weight loss after only 7h 30 min.

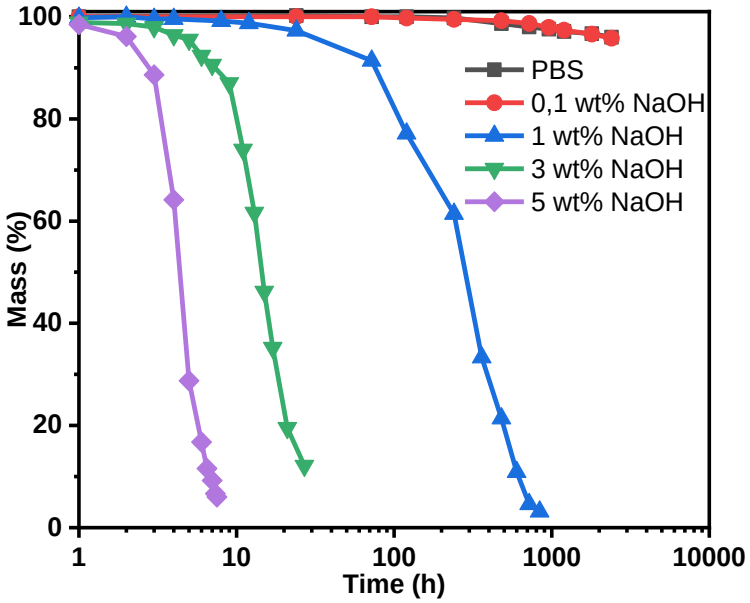

Figure 8. Mass % evolution of MDO-based biporous scaffolds Bi80S80 depending on the hydrolytic conditions.

Table 6. Kinetic parameters for biporous MDO-based scaffold Bi80S80 hydrolysis in different media.

Medium	pH	k (h^{-1})	R^2	R^2_{adj}
PBS	7.4	$1.61.10^{-5}$	0.894	0.873
0.1 wt.% NaOH	12.4	$1.83.10^{-5}$	0.980	0.977
1 wt.% NaOH	13.4	$4.55.10^{-3}$	0.982	0.979
3 wt.% NaOH	13.9	$1.16.10^{-1}$	0.989	0.986
5 wt.% NaOH	14.0	$6.57.10^{-1}$	0.995	0.994

4. Conclusions

In the present work, we reported the preparation of a novel hierarchically structured biporous MDO-based network with well-defined porous morphology by the double porogen templating approach as confirmed by SEM and MIP. It was shown that the dual porosity enhanced the elastic behavior during compressibility of the materials which was also tuned by the variation of the crosslinking agent, the increase in crosslink density increasing the elastic modulus. In addition, these materials possessed unique absorption properties as a synergic effect was observed on water uptake for biporous materials compared to the monoporous analogues, thus confirming a high interconnectivity of the structure. MDO-based materials were stable under PBS after 100 days; however, a fast degradation was observed under alkaline accelerated conditions due to the facile hydrolysis of the ester functionalities on the polymeric backbone. Therefore, these novel MDO-based biporous scaffolds constitute promising candidates for their application in tissue engineering as an alternative to the commonly used polymers (PCL, PLA, PGA, *etc.*), as they may be highly functionalized by insertion of other functional comonomers, such as vinyl ethers. Ongoing research is focusing on the insertion of functional comonomers to achieve post-polymerization functionalization of such porous polymers with bio-relevant molecules in a straightforward way under mild conditions.

References

[1] G.C. Gurtner, M.J. Callaghan, M.T. Longaker, Progress and Potential for Regenerative Medicine, Annu. Rev. Med. 58 (2007) 299–312. https://doi.org/10.1146/annurev.med.58.082405.095329.

[2] F.-M. Chen, X. Liu, Advancing biomaterials of human origin for tissue engineering, Prog. Polym. Sci. 53 (2016) 86–168. https://doi.org/10.1016/j.progpolymsci.2015.02.004.

[3] B.D. Ratner, A pore way to heal and regenerate: 21st century thinking on biocompatibility, Regen. Biomater. 3 (2016) 107–110. https://doi.org/10.1093/rb/rbw006.

[4] L.M. Koh, S.M. Khor, Current state and future prospects of sensors for evaluating polymer biodegradability and sensors made from biodegradable polymers: A review, Anal. Chim. Acta 1217 (2022) 339989. https://doi.org/10.1016/j.aca.2022.339989.

[5] F.J. O'Brien, Biomaterials & scaffolds for tissue engineering, Mater. Today 14 (2011) 88–95. https://doi.org/10.1016/S1369-7021(11)70058-X.

[6] J.L. Hernandez, K.A. Woodrow, Medical Applications of Porous Biomaterials: Features of Porosity and Tissue- Specific Implications for Biocompatibility, Adv. Healthc. Mater. 11 (2022) 2102087. https://doi.org/10.1002/adhm.202102087.

[7] V. Karageorgiou, D. Kaplan, Porosity of 3D biomaterial scaffolds and osteogenesis, Biomaterials 26 (2005) 5474–5491. https://doi.org/10.1016/j.biomaterials.2005.02.002.

[8] D. Jeyachandran, M. Cerruti, Glass, Ceramic, Polymeric, and Composite Scaffolds with Multiscale Porosity for Bone Tissue Engineering, Adv. Eng. Mater. 25 (2023) 2201743. https://doi.org/10.1002/adem.202201743.

[9] Y. Zhao, K. Tan, Y. Zhou, Z. Ye, W.-S. Tan, A combinatorial variation in surface chemistry and pore size of three-dimensional porous poly(ε-caprolactone) scaffolds modulates the behaviors of mesenchymal stem cells, Mater. Sci. Eng. C 59 (2016) 193–202. https://doi.org/10.1016/j.msec.2015.10.017.

[10] N. Yuan, W. Tian, L. Sun, R. Yuan, J. Tao, D. Chen, Neural stem cell transplantation in a double-layer collagen membrane with unequal pore sizes for spinal cord injury repair, Neural Regen. Res. 9 (2014) 1014. https://doi.org/10.4103/1673-5374.133160.

[11] C.G. Jeong, S.J. Hollister, Mechanical and Biochemical Assessments of Three-Dimensional Poly(1,8-Octanediol-co-Citrate) Scaffold Pore Shape and Permeability Effects on In Vitro Chondrogenesis Using Primary Chondrocytes, Tissue Eng. Part A 16 (2010) 3759–3768. https://doi.org/10.1089/ten.tea.2010.0103.

[12] M. Ebrahimi, Porosity parameters in biomaterial science: Definition, impact, and challenges in tissue engineering, Front. Mater. Sci. 15 (2021) 352–373. https://doi.org/10.1007/s11706-021-0558-4.

[13] D. Lu, Z. Zeng, Z. Geng, C. Guo, D. Pei, J. Zhang, S. Yu, Macroporous methacrylated hyaluronic acid hydrogel with different pore sizes for in vitro and in vivo evaluation of vascularization, Biomed. Mater. 17 (2022) 025006. https://doi.org/10.1088/1748-605X/ac494b.

[14] K. Zhang, Y. Fan, N. Dunne, X. Li, Effect of microporosity on scaffolds for bone tissue engineering, Regen. Biomater. 5 (2018) 115–124. https://doi.org/10.1093/rb/rby001.

[15] C.Y. Beh, E.M. Cheng, N.F. Mohd Nasir, M.S. Abdul Majid, M.R. Mohd Roslan, K.Y. You, S.F. Khor, M.J. M Ridzuan, Fabrication and characterization of three-dimensional porous cornstarch/n-HAp biocomposite scaffold, Bull. Mater. Sci. 43 (2020) 249. https://doi.org/10.1007/s12034-020-02217-0.

[16] Q. Yao, Y. Liu, Y. Pan, J.M. Miszuk, H. Sun, One- pot porogen free method fabricated porous microsphere- aggregated 3D PCL scaffolds for bone tissue engineering, J.

Biomed. Mater. Res. B Appl. Biomater. 108 (2020) 2699–2710. https://doi.org/10.1002/jbm.b.34601.
[17] C. Tao, Y. Zhang, B. Li, L. Chen, Hierarchical micro/submicrometer-scale structured scaffolds prepared via coaxial electrospinning for bone regeneration, J. Mater. Chem. B 5 (2017) 9219–9228. https://doi.org/10.1039/C7TB02044A.
[18] C. Zhou, K. Yang, K. Wang, X. Pei, Z. Dong, Y. Hong, X. Zhang, Combination of fused deposition modeling and gas foaming technique to fabricated hierarchical macro/microporous polymer scaffolds, Mater. Des. 109 (2016) 415–424. https://doi.org/10.1016/j.matdes.2016.07.094.
[19] D. Gupta, P. Vashisth, J. Bellare, Multiscale porosity in a 3D printed gellan–gelatin composite for bone tissue engineering, Biomed. Mater. 16 (2021) 034103. https://doi.org/10.1088/1748-605X/abf1a7.
[20] S. Mezhoud, B. Le Droumaguet, P. Aimedieu, V. Monchiet, M. Bornert, D. Grande, Investigation of morphology associated with biporous polymeric materials obtained by the double porogen templating approach, Colloid Polym. Sci. 299 (2021) 537–550. https://doi.org/10.1007/s00396-020-04747-9.
[21] H.B. Ly, B. Le Droumaguet, V. Monchiet, D. Grande, Facile fabrication of doubly porous polymeric materials with controlled nano- and macro-porosity, Polymer 78 (2015) 13–21. https://doi.org/10.1016/j.polymer.2015.09.048.
[22] H.B. Ly, R. Poupart, B. Carbonnier, V. Monchiet, B. Le Droumaguet, D. Grande, Versatile functionalization platform of biporous poly(2-hydroxyethyl methacrylate)-based materials: Application in heterogeneous supported catalysis, React. Funct. Polym. 121 (2017) 91–100. https://doi.org/10.1016/j.reactfunctpolym.2017.10.024.
[23] M.A. Woodruff, D.W. Hutmacher, The return of a forgotten polymer—Polycaprolactone in the 21st century, Prog. Polym. Sci. 35 (2010) 1217–1256. https://doi.org/10.1016/j.progpolymsci.2010.04.002.
[24] H. Hajiali, Shahgasempour, M.R. Naimi-Jamal, Peirovi, Electrospun PGA/gelatin nanofibrous scaffolds and their potential application in vascular tissue engineering, Int. J. Nanomedicine (2011) 2133. https://doi.org/10.2147/IJN.S24312.
[25] E.H. Backes, E.M. Fernandes, G.S. Diogo, C.F. Marques, T.H. Silva, L.C. Costa, F.R. Passador, R.L. Reis, L.A. Pessan, Engineering 3D printed bioactive composite scaffolds based on the combination of aliphatic polyester and calcium phosphates for bone tissue regeneration, Mater. Sci. Eng. C 122 (2021) 111928. https://doi.org/10.1016/j.msec.2021.111928.
[26] D. Zhao, T. Zhu, J. Li, L. Cui, Z. Zhang, X. Zhuang, J. Ding, Poly(lactic-co-glycolic acid)-based composite bone-substitute materials, Bioact. Mater. 6 (2021) 346–360. https://doi.org/10.1016/j.bioactmat.2020.08.016.
[27] N. Siddiqui, S. Asawa, B. Birru, R. Baadhe, S. Rao, PCL-Based Composite Scaffold Matrices for Tissue Engineering Applications, Mol. Biotechnol. 60 (2018) 506–532. https://doi.org/10.1007/s12033-018-0084-5.
[28] P. Plikk, T. Tyson, A. Finne- Wistrand, A. Albertsson, Mapping the characteristics of the radical ring- opening polymerization of a cyclic ketene acetal towards the creation of a functionalized polyester, J. Polym. Sci. Part Polym. Chem. 47 (2009) 4587–4601. https://doi.org/10.1002/pola.23511.
[29] W.J. Bailey, Z. Ni, S.-R. Wu, Synthesis of poly-ε-caprolactone via a free radical mechanism. Free radical ring-opening polymerization of 2-methylene-1,3-dioxepane, J. Polym. Sci. Polym. Chem. Ed. 20 (1982) 3021–3030. https://doi.org/10.1002/pol.1982.170201101.
[30] T.L.D.A. Montanheiro, L.S. Montagna, V. Patrulea, O. Jordan, G. Borchard, R.G. Ribas, T.M.B. Campos, G.P. Thim, A.P. Lemes, Enhanced water uptake of PHBV scaffolds with

functionalized cellulose nanocrystals, Polym. Test. 79 (2019) 106079. https://doi.org/10.1016/j.polymertesting.2019.106079.
[31] F.-C. Wu, R.-L. Tseng, R.-S. Juang, Initial behavior of intraparticle diffusion model used in the description of adsorption kinetics, Chem. Eng. J. 153 (2009) 1–8. https://doi.org/10.1016/j.cej.2009.04.042.
[32] E.D. Revellame, D.L. Fortela, W. Sharp, R. Hernandez, M.E. Zappi, Adsorption kinetic modeling using pseudo-first order and pseudo-second order rate laws: A review, Clean. Eng. Technol. 1 (2020) 100032. https://doi.org/10.1016/j.clet.2020.100032.
[33] J. Bujdák, Adsorption kinetics models in clay systems. The critical analysis of pseudo-second order mechanism, Appl. Clay Sci. 191 (2020) 105630. https://doi.org/10.1016/j.clay.2020.105630.
[34] H.-B. Ly, B. Le Droumaguet, V. Monchiet, D. Grande, Designing and modeling doubly porous polymeric materials, Eur. Phys. J. Spec. Top. 224 (2015) 1689–1706. https://doi.org/10.1140/epjst/e2015-02491-x.
[35] B. Le Droumaguet, R. Lacombe, H.-B. Ly, M. Guerrouache, B. Carbonnier, D. Grande, Engineering functional doubly porous PHEMA-based materials, Polymer 55 (2014) 373–379. https://doi.org/10.1016/j.polymer.2013.08.067.
[36] A. Tardy, J. Nicolas, D. Gigmes, C. Lefay, Y. Guillaneuf, Radical Ring-Opening Polymerization: Scope, Limitations, and Application to (Bio)Degradable Materials, Chem. Rev. 117 (2017) 1319–1406. https://doi.org/10.1021/acs.chemrev.6b00319.
[37] A. Tardy, J. Honoré, J. Tran, D. Siri, V. Delplace, I. Bataille, D. Letourneur, J. Perrier, C. Nicoletti, M. Maresca, C. Lefay, D. Gigmes, J. Nicolas, Y. Guillaneuf, Radical Copolymerization of Vinyl Ethers and Cyclic Ketene Acetals as a Versatile Platform to Design Functional Polyesters, Angew. Chem. Int. Ed. 56 (2017) 16515–16520. https://doi.org/10.1002/anie.201707043.
[38] F. Wenzel, S. Hamzehlou, L. Pardo, M. Aguirre, J.R. Leiza, Kinetics of Radical Ring Opening Polymerization of the Cyclic Ketene Acetal 2-Methylene-1,3-dioxepane with Vinyl Monomers, Ind. Eng. Chem. Res. 60 (2021) 10479–10488. https://doi.org/10.1021/acs.iecr.0c04117.
[39] S. Agarwal, R. Kumar, T. Kissel, R. Reul, Synthesis of Degradable Materials Based on Caprolactone and Vinyl Acetate Units Using Radical Chemistry, Polym. J. 41 (2009) 650–660. https://doi.org/10.1295/polymj.PJ2009091.
[40] A. Tardy, N. Gil, C.M. Plummer, C. Zhu, S. Harrisson, D. Siri, J. Nicolas, D. Gigmes, Y. Guillaneuf, C. Lefay, DFT-calculation-assisted prediction of the copolymerization between cyclic ketene acetals and traditional vinyl monomers, Polym. Chem. 11 (2020) 7159–7169. https://doi.org/10.1039/D0PY01179G.
[41] G.G. Hedir, C.A. Bell, N.S. Ieong, E. Chapman, I.R. Collins, R.K. O'Reilly, A.P. Dove, Functional Degradable Polymers by Xanthate-Mediated Polymerization, Macromolecules 47 (2014) 2847–2852. https://doi.org/10.1021/ma500428e.
[42] B.G. Zadontsev, V.G. Neroznik, O.I. Vasilova, T.V. Novikova, S.I. Kuznetsova, Yu.S. Zaitsev, Kinetic patterns of the synthesis and aspects of the structure of styrene copolymers with divinyl adipate, Polym. Sci. USSR 26 (1984) 1777–1782. https://doi.org/10.1016/0032-3950(84)90352-6.
[43] W.J. Bailey, T. Endo, B. Gapud, Y.-N. Lin, Z. Ni, C.-Y. Pan, S.E. Shaffer, S.-R. Wu, N. Yamazaki, K. Yonezawa, Synthesis of Functionally-Terminated Oligomers by Free Radical Ring-Opening Polymerization, J. Macromol. Sci. Part - Chem. 21 (1984) 979–995. https://doi.org/10.1080/00222338408056586.
[44] K. Chuda, J. Jasik, J. Carlier, P. Tabourier, C. Druon, X. Coqueret, Characteristics and fluidic properties of porous monoliths prepared by radiation-induced polymerization for

Lab-on-a-Chip applications, Radiat. Phys. Chem. 75 (2006) 26–33. https://doi.org/10.1016/j.radphyschem.2005.06.007.
[45] H. Fukuda, M. Hirota, T. Endo, Relationship between reaction rates and NMR chemical shifts in the reaction of cyclic ketene acetals with methanol, Tetrahedron Lett. 27 (1986) 1587–1590. https://doi.org/10.1016/S0040-4039(00)84321-X.
[46] B.R. Kordes, L. Ascherl, C. Rüdinger, T. Melchin, S. Agarwal, Competition between Hydrolysis and Radical Ring-Opening Polymerization of MDO in Water. Who Makes the Race?, Macromolecules 56 (2023) 1033–1044. https://doi.org/10.1021/acs.macromol.2c01653.
[47] Q. Yang, J. Xue, W. Li, X. Du, Q. Ma, K. Zhan, Z. Chen, Comprehensive evaluation and interpretation of mercury intrusion porosimetry data of coals based on fractal theory, Tait equation and matrix compressibility, Fuel 298 (2021) 120823. https://doi.org/10.1016/j.fuel.2021.120823.
[48] T. Tadros, Flory-Huggins Interaction Parameter, in: T. Tadros (Ed.), Encycl. Colloid Interface Sci., Springer Berlin Heidelberg, Berlin, Heidelberg, 2013: pp. 523–524. https://doi.org/10.1007/978-3-642-20665-8_89.
[49] A.F.M. Barton, CRC handbook of polymer-liquid interaction parameters and solubility parameters, CRC Press, Boca Raton, 1990.
[50] C. Etxabarren, M. Iriarte, C. Uriarte, A. Etxeberría, J.J. Iruin, Polymer–solvent interaction parameters in polymer solutions at high polymer concentrations, J. Chromatogr. A 969 (2002) 245–254. https://doi.org/10.1016/S0021-9673(02)00886-5.
[51] J. Brandup, E.H. Immergut, E.A. Grulke, eds., Polymer Handbook, 4th ed., John Wiley and Sons, New York, 1999. https://onlinelibrary.wiley.com/doi/10.1002/1097-0126(200007)49:7<807::AID-PI436>3.0.CO;2-1 (accessed January 25, 2024).
[52] S. Diamond, Mercury porosimetry: An inappropriate method for the measurement of pore size distributions in cement-based materials, Cem. Concr. Res. 30 (2000) 1517–1525. https://doi.org/10.1016/S0008-8846(00)00370-7.
[53] A.S.P. Lin, T.H. Barrows, S.H. Cartmell, R.E. Guldberg, Microarchitectural and mechanical characterization of oriented porous polymer scaffolds, Biomaterials 24 (2003) 481–489. https://doi.org/10.1016/S0142-9612(02)00361-7.
[54] O. Okay, Macroporous copolymer networks, Prog. Polym. Sci. 25 (2000) 711–779. https://doi.org/10.1016/S0079-6700(00)00015-0.
[55] B.-S. Chiou, P.E. Schoen, Effects of crosslinking on thermal and mechanical properties of polyurethanes, J. Appl. Polym. Sci. 83 (2002) 212–223. https://doi.org/10.1002/app.10056.
[56] A. Löfgren, A.-C. Albertsson, Copolymers of 1,5-dioxepan-2-one and L- or D,L-dilactide: Hydrolytic degradation behavior, J. Appl. Polym. Sci. 52 (1994) 1327–1338. https://doi.org/10.1002/app.1994.070520917.